Development of a Hyperspectral Colposcope for Early Detection and Assessment of Cervical Dysplasia

Carlos Vega[1], Raquel Leon[1], Norberto Medina[2], Himar Fabelo[1,3], Samuel Ortega[1,5], Fran Balea [1,4], Aday García[2], Margarita Medina[2], Silvia de León[2], Alicia Martín[2], Gustavo M. Callico[1]
[1]*Research Institute for Applied Microelectronics (IUMA), University of Las Palmas de Gran Canaria (ULPGC), Las Palmas de Gran Canaria, Spain*
[2] *Complejo Hospitalario Universitario Insular Materno Infantil (CHUIMI), Servicio Canario de Salud (SCS), Las Palmas de Gran Canaria, Spain*
[3] *Fundación Canaria Instituto de Investigación Sanitaria de Canarias (FIISC), Las Palmas de Gran Canaria, Spain*
[4] *Dept. of Psychology, Sociology and Social Work, Universidad de Las Palmas de Gran Canaria, Las Palmas de Gran Canaria (ULPGC), Spain*
[5] *Norwegian Institute of Food, Fisheries and Aquaculture Research (Nofima), Tromsø, Norway*
cvega@iuma.ulpgc.es

Abstract—The early detection of precancerous cervical lesions is essential to improve patient treatment and prognosis. Current methods of screening and diagnosis have improved the detection of these lesions but still present some critical limitations. Hyperspectral (HS) imaging is emerging as a new non-invasive and label-free imaging technique in the medical field for performing quick diagnosis of different diseases. This work describes the first step in the research and development process to present to the gynaecologist a new non-invasive tool to detect cervical neoplasia during routine medical procedures. This tool is based on a HS camera coupled to a colposcope, a primary tool already used in cervical examinations. The developed HS colposcope was validated by comparing the HS images obtained against the captures obtained with conventional optics. Results show the feasibility of the developed system to start a data acquisition campaign of cervical lesions targeting future developments of algorithms based on artificial intelligence.

Keywords—hyperspectral imaging instrumentation; Cervical intraepithelial neoplasia (CIN); cervical cancer; image processing

I. INTRODUCTION

Cervical cancer ranks seventh in incidence and ninth mortality worldwide, with a growing incidence in 2020 of 604,127 new cases (13.3 cases/100,000 women-year) [1]. When referring to women under 45 years of age, it represents the second most common cancer, after breast cancer, with a rate of 5.7 cases per 100,000 women-year [2]. However, in Spain, cervical cancer for all ages ranks ninth in incidence in women, reaching fourth place in women under 45 years of age [3]. The Autonomous Community of the Canary Islands shows one of the highest incidences in the national territory, with a gross rate of 11.5 per 100,000 women-year in 2018. In the province of Las Palmas, the cervical cancer rate is 10 cases per 100,000 women-year, of which 24% correspond to women under 45 years of age [3]. These data show the need of developing new tools for screening and early detection of cervical cancer.

Invasive squamous epithelial carcinoma of the cervix develops from precursor lesions determined high-grade squamous Cervical Intraepithelial Neoplasia (CIN 3). The necessary but not sufficient condition for the onset of this pathology is the persistence of infection by the Human Papilloma Virus (HPV) [4]. The natural history of cervical cancer started several years or decades earlier, with HPV infection in the keratinocytes of the basal stratum of the squamous epithelium. This process begins with low-grade benign lesions that progress to squamous cell high-grade lesions with a high potential for malignancy [5]. The destruction and involvement of the lower third is called CIN 1, a benign lesion that regresses spontaneously in 60% of cases. When the degree of involvement of the squamous epithelium affects two thirds, which is called inferior CIN 2, the lesion is already labelled as high-grade.

The early detection of a possible CIN is performed by a Papanicolaou test (Pap smear) [6]. This is a method of cervical primary screening for detecting potentially precancerous and cancerous lesions in the cervix. It is permed by collecting cells from the cervix with a cytobrush and a posterior examination of the samples under a microscope [7]. Once a test indicates abnormal results, the patient must undergo a colposcopy evaluation. This evaluation, in combination with colposcopic biopsies, is critical to decide about returning patient to routine screening, more intensive surveillance, or treatment [8]. During this process, the gynaecologist examines the cervix with a colposcope with a white or green light source. Also, it is common to apply acid acetic or Lugol's Iodine to facilitate the diagnosis [9].

This method of screening and diagnosis is widely accepted, but has some limitations, such as the low sensitivity of the Pap smear test [10] and the poor specificity of the colposcopy for localising cervical neoplasia [8], [11]. Globally, this often leads to perform unnecessary biopsies [12]. These limitations motivate the use of new technologies for improving sensitivity and specificity of cervical cancer screening and early detection.

Hyperspectral Imaging (HSI), also known as imaging spectroscopy, is an emerging technology in the medical field that integrates conventional image and spectroscopy methods for obtaining spatial and spectral information from the captured scene [13]. Hyperspectral (HS) images differ from standard red, green, and blue (RGB) or multispectral images (which have a few more bands than the RGB image) by capturing a wide range of the electromagnetic spectrum with the ability of acquiring a large number of contiguous and narrow spectral bands. The HS cameras measure the intensity of light reflected, absorbed, or emitted in specific wavelengths by the materials of the sample.

Several studies have been conducted to evaluate the use of spectroscopy and HSI on in-vivo CIN diagnosis. In 2002, reflectance spectroscopy for in-vivo detection of cervical cancer was studied using a spectrograph in the wavelength range between 355 nm and 655 nm in increments of 2.5 nm [14]. Wang *et al.* studied the application of spectroscopy in the uterine-cervical epithelial tissue in 2004 with an approach based on Monte Carlo simulations. Their work obtained from the simulations that the bands with more significant variability in the spectral signatures of the different tissues were the Soret

2771-2508/22/$31.00 ©2022 IEEE
DOI 10.1109/DSD57027.2022.00121

(420 nm) and the Q-band (540 – 580 nm) [15]. In 2016, a preliminary study presented the use of multi-scale HSI for detecting cervical neoplasia at tissue and cellular levels [16]. HS images were captured with an industrial camera, attached to an Acousto-Optic Tuneable Filter (AOTF) with a filtering range between 500 and 900 nm, with an FWHM (Full Width at Half Maximum) for each band of 2 nm. The samples were captured in-vivo, with the patient examination, and ex-vivo, from tissue slices in the microscope. Results were promising for both types of data by utilising HS data between 600 and 800 nm, which is even outside the previous more relevant range. These previous studies show promising results in the application of HSI to detect CIN, which, as explained before, are the lesions that precede the development of cervical cancer. Furthermore, the promising results of HSI in diagnosing other cancer diseases and in medical-guided surgery [17] support the importance of developing new tools for cervical examination with HSI capabilities.

The goal of this work is the development of a non-invasive and label-free HS colposcope for facilitating the detection of cervical neoplasia during routine medical procedures. The long-term objective is to generate a precise delineation of the lesion's extension in real-time and the identification of the different grade areas to avoid the resection of normal cervical tissue, which is a challenging task in current surgical operations. So, to extend the physician's visual capabilities and overcome previous limitations, we propose to use HSI.

II. Materials and Methods

This section describes the necessary materials and the methods followed to perform the integration of the HS-based acquisition system and its technical validation.

A. Elements of the Acquisition System

1) Hyperspectral Camera

The acquisition system must obtain the necessary information for detecting the CIN in its different grades. It is essential to know the spectral range where the samples' spectral signatures are more characterizable. As analysed in the introduction, the previous works on spectroscopy and HSI for cervical diagnosis were based on various spectral ranges. The most recent is based on the diagnostics in the spectral range between 600 nm and 800 nm [16], but [15] established the Q-band (540 – 580 nm) and the Soret Band (420 nm) as the most relevant for identifying the different cervical tissues.

Due to this diversity of spectral ranges between the previous studies, the HS camera Snapscan VNIR (IMEC, Belgium) was chosen, which covers the 470 to 900 nm spectral range. This camera is based on a spatio-spectral scanning technology called *Snapscan* [18].

This technology works by the movement of the sensor inside the camera. There is a Gaussian filter over each sensor column, which only allows capturing one spectral band. The spectral cube is obtained by taking a series of frames in which each of them captures a diagonal plane of the HS cube. The capture process is shown in Fig. 1, with each frame captured indicated with the t_n representation. In the figure, it is represented the HS cube with half of the data acquired. The frame t_4 (in the middle) is captured when the sensor is in the middle of its range of movement, so a diagonal plane is captured, covering all the spatial area but with each Y column shifted one spectral band from the adjacent ones. All the previous frames are captured in the same way, but with the sensor shifted on the X-axis. This movement causes that in these frames, just part of the sensor adds new information to the cube. For example, in the first frame, t_0, the sensor is positioned on one side of the X-axis, so just the last cube column in the lowest wavelength is captured [19]. In the example, the cube is represented with a small size, but the IMEC Snapscan can generate a cube of 3,650 columns by 2,048 rows and 150 spectral bands. The dimensions can be reduced, as it has a relevant impact on the acquisition time.

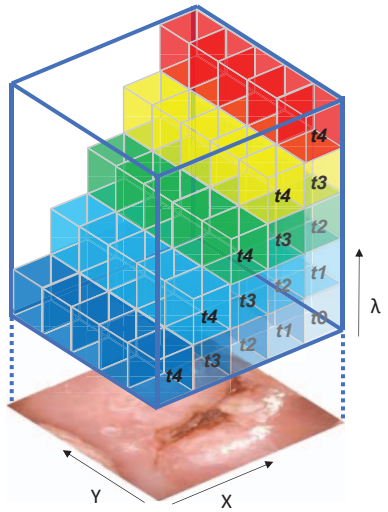

Fig. 1. Representation of the spatio-spectral HSI scanning used in the IMEC Snapscan HS camera.

The main benefit of the spatio-spectral technology is its trade-off between a fast acquisition time and a high spectral and spatial resolution. These characteristics make this technology very convenient for our project, as it is crucial to keep the acquisition time as short as possible to avoid any inconveniences in the gynaecologist's workflow or in the patient, who needs to remain still during the capture. There is a faster imaging technique, called *snapshot*, which is able to capture all the bands in one single shot, but usually involves a high trade-off between its spatial and spectral resolution [17].

2) Colposcope

The colposcope is a type of microscope with stereoscopic binocular vision and low magnification combined with a light source. This tool allows the doctor to visualize with high detail any abnormal region in the cervix and decide if it is necessary to perform a biopsy of the area and send it to the pathologist to obtain a definitive diagnosis of the lesion.

For this work, the Optomic OP-C2 (Optomic, Spain) colposcope was used. This colposcope is a common model used in many medical offices and is characterised by having a modular design. The device is divided into three main parts: the head (Fig. 2.A and B), the image splitter (Fig. 2.C) and the binoculars (Fig. 2.E). This model has an infrared filter on the front, which had to be removed explicitly by the manufacturer to allow the HS camera to capture data in its whole spectral range.

3) Illumination System

The colposcope includes an external light source that transmits the light to the head by a fibre optic light guide. This light source is based on LED (Light-Emitting Diode) technology, which produces a powerful white light source. It

also includes a green filter that is used to facilitate the diagnosis in combination with Lugol's Iodine. Nevertheless, the original LED-based light source was not a valid solution for HSI utilisation because of the narrow spectral range of emission. Then, in this work, we modified the light source and employed the Techniquip Model 21DC (TechniQuip, Pleasanton, CA, USA) which is based on a halogen bulb with a constant DC (Direct Current) power regulator.

The light source is connected to the colposcope by a fibre optic light guide from Karl Storz (Germany), specifically the model 81594 SB. This model is a high-performance fibre from the manufacturer, with an internal diameter of 5 mm and a length of 250 mm.

B. System Integration

The proposed system must be usable in the current workflow of the gynaecologist. This implies that everything must be integrated robustly, reducing any possible problems during its usage. Our goal is to integrate the HS camera with the current colposcopes present in the gynaecologist's office and the RGB camera.

The first step was the coupling between the HS camera (Fig. 2.D) and the splitter (Fig. 2.C). Both devices had a connection based on the C-mount standard, but since the HS camera has a larger volume and weight than the original RGB camera, it was necessary to design an external bracket. As shown in Fig. 2, the camera is placed vertically in relation to the colposcope. The bracket (Fig. 2.C) connects the HS camera body to the colposcope's splitter. It is coupled to the camera by two screws and to the splitter with its shape and one screw.

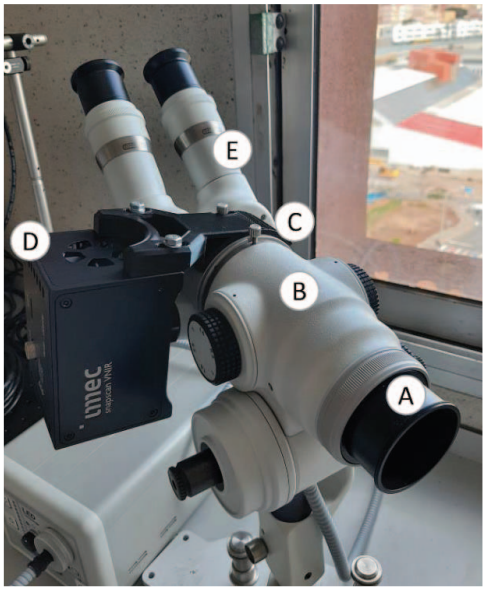

Fig. 2. Bracket between IMEC Snapscan and colposcope on the initial tests without the RGB camera. A) front lenses; B) main body; C) image splitter and bracket; D) HS camera; E) binoculars.

One issue presented with this configuration was that the focal distance for the camera was slightly offset. The HS camera connects with C-mount standard, which has a flange focal distance of 17.526 mm, while the splitter is prepared for the standard CS-mount, which has the same thread diameter (25.4 mm) and thread step (32 threads per inch), but the flange focal distance is reduced to 12.526 mm. This offset in the focal distance of 5 mm causes that, if the system is focused for seeing with binoculars, the camera is not entirely focused and vice versa. To solve this problem, the camera was focused with a reference object, and the binoculars were compensated with the graduation for the vision problems until the object was also focused. However, when the RGB camera is also included, the system must be focused as usual with the RGB and binocular. Next the gynaecologist must refocus the colposcope to capture an image with the HS camera. It is inconvenient for its use, but it will be corrected in future versions by adjusting the focus lens in the HS camera splitter.

The connection between the HS camera and the computer must be adapted to the shape and space available on the colposcope. As shown in Fig. 3, the colposcope is held with a custom arm that allows easy movement and locking it in a specific position. Over the arm, it is placed the screen, which allows the gynaecologist to interact with the Graphical User Interface (GUI).

The HS camera has two connections. The first one is the data connection by USB 3.0 that connects directly to the computer (PC). The second connection is a custom interface that includes the power lines and the camera's control. This is connected to an independent camera controller, which is placed over the lower arm of the colposcope's support (Fig. 3) and it is connected to the PC by USB 2.0.

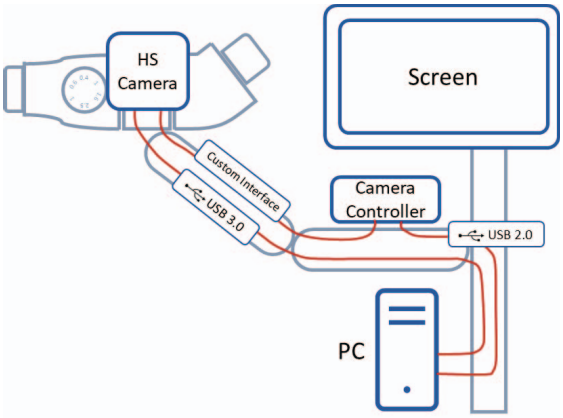

Fig. 3. Schematic Connection on Colposcope

C. HS Reference samples and acquisition

As a baseline, different reference samples were captured with the camera manufacturer's acquisition system setup (Fig. 4). The same reference samples were captured with the HS colposcope in order to compare both HS images to identify whether the colposcope introduced distortion in the HS images. The reference setup is composed of a main structure (Fig. 4.A), four halogen spotlights (Fig. 4.B), a power supply (Fig. 4.C), and the HS camera (Fig. 4.D). The structure holds the four halogen spotlights that illuminate the sample, and the HS camera is placed on the top. Different parts of the system can be adjusted, as is a modular design. In this case, the HS camera was adjusted to a distance of 320 mm from the base during the captures. The lens included with the reference kit is the Apo-Xenoplan 2.0/24 4 (Schneider Optics, Hauppauge, NY, USA). This lens offers a manually adjustable iris and focus, which was sufficient for the tests. Finally, during the capture of the images, external illumination of the room was reduced to avoid any possible distortion in the results.

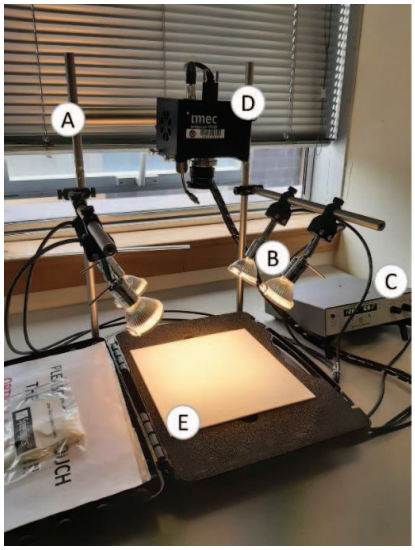

Fig. 4. Reference HS acquisition system setup for the IMEC Snapscan VNIR camera. A) structure B) halogen illumination C) power supply D) HS camera E) white reference

In order to identify any spatial or spectral distortion introduced by the colposcope and illumination system, different reference samples were captured with the HS colposcope and compared to the HS images captured by the reference HS camera system.

The Zenith Lite Diffuse Target SG3151, manufactured by SphereOptics (Germany), which provides a surface of 200 × 200 mm with a high reflectance, up to 95%, with nearly ideal diffuse Lambertian reflectance over the wavelengths between 250 and 2500 nm. This target was used as white reference, necessary to perform the HS image calibration (Fig. 4.E). This HS image was captured before starting the capturing process. This reduces the spectral deformation caused by the spectral characteristics of the light source and the camera's different sensitivity to each wavelength. The calibration process is performed automatically by the IMEC's software after capturing the HS image. In addition, this target was used to perform different experiments.

The Zenith Polymer Diffuse Reflectance SG3333 (SphereOptics, Germany) was used as spectral reference (Fig. 5.A). This material is a mixture of three pure, rare-earth oxides of Holmium, Erbium and Dysprosium mixed into the Zenith Polymer. It exhibits distinct absorption peaks, which will be used to compare any distortion introduced by the acquisition system. The manufacturer provides the calibrated spectrum signature for this material in the range between 250 to 2450 nm in steps of 0.1 nm.

For analysing spatial deformations introduced by the HS colposcope, a distortion target manufactured by Edmund Optics (NJ, USA) was used (Fig. 5.B). This reference allows for determining the precise amount of distortion present in the system by measuring the distances between its dots. The patterns are organised in five squares with variable frequency and size of the dots between them. This sample differs from the traditional used in optics by its composition. The base is made from opal glass, which offers a constant reflection figure on our sensor's spectrum capture range. At the same time, the pattern is manufactured with vacuum deposited chromium oxide. The utilisation of these materials allows for capturing a clear image of the pattern in each of the spectral bands.

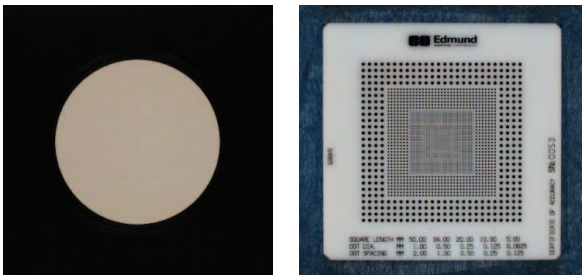

(A) (B)

Fig. 5. Image of the reference objects captured on the reference system. A) Zenith Polymer SG3333; B) Edmunds Distortion Target.

D. Graphical User Interface (GUI)

The GUI was developed to simplify the data capture process in the clinical environment. The development was carried out based on the Application Program Interface (API) from the camera's manufacturer (Fig. 6), which gives access to the camera's functionalities.

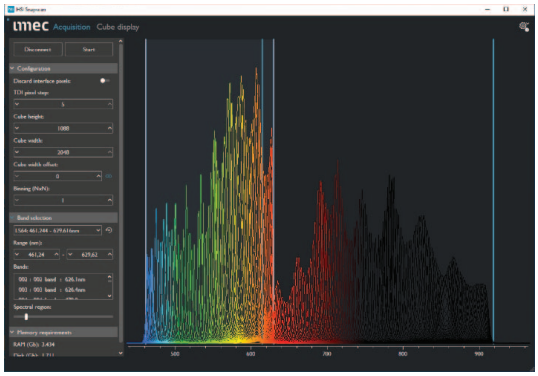

Fig. 6. HSI Snapscan (camera manufacturer GUI) in the initial configuration screen.

The main improvement over the camera manufacturer's acquisition software is the abstraction from the low-level configuration parameters. Fig. 7 shows a capture of the developed GUI. The main actions of the system are located at the top of the application (A). The live view is located in the centre (B), which helps the clinician visualise the camera's vision area and focus the system. Finally, on the right part (C), there is the new patient area where the gynaecologist set the patient's identifier.

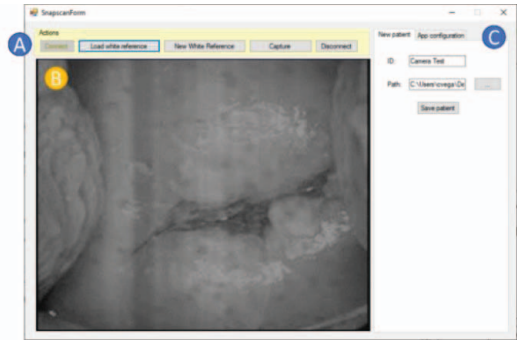

Fig. 7. GUI with an example of a reference cervical image. A) Area with main capture actions; B) Live view; C) area for indicating the user id and save folder path.

The process for capturing an image was also simplified from the manufacturer's process by removing the repetitive configuration steps and by loading default references, instead of capturing one each time. Initially, the system must be configured by a technician who has to fine-tune the exposure time, adjust any offset in the image, set the specific compensation file for the camera unit and capture the white reference. Once this process is completed, the medical doctor just has to follow the next procedure:

1. **Connect the camera:** the software connects to the camera, load the configuration and starts capturing the image in the live view. If the camera is going to be constantly used, this only needs to be done when the system is initially turned on.
2. **Set the patient ID:** When the ID is set, the software creates a folder with the current date and the ID. In this folder, the system will save all the captures done in the process.
3. **Capture or load a white reference:** The software automatically loads the default *White Reference*, as it is not necessary to capture the white reference before each image. If the system needs to be recalibrated, the user can capture a new one or load it from a file.
4. **Capture the HS cube:** At this stage, the medical doctor just needs to click on the capture button and wait until the image is saved. Before pressing this button, it is important to ensure that the sample is correctly focused. When it finishes, the medical doctor can keep taking more pictures or change the patient's ID.
5. **Disconnect:** This does not need to be done constantly, just when the system is not going to be used anymore.

III. Experimental Results and Discussion

A. Comparison results with the reference system setup

The validation of the proposed HS colposcope was performed by analysing the results obtained with the proposed solution in relation to the ones obtained with the reference HS acquisition system setup. The captured samples were the reference objects described in Section II.C. All the image processing steps were performed using MATLAB® R2022a (The MathWorks, MA, USA) software environment.

1) Experiment with the Polymer SG3333

The Zenith Polymer SG3333 was used to compare the spectral performance. Fig. 8 shows the average spectral signature of the SG3333 captured using the reference HS camera system (in blue), the proposed system (in red), and the certified spectral signature provided by the SG3333 manufacturer (in green). It is noticeable that the spectral signatures are similar to the reference, in the capture spectral range, but lack the small spectral peaks that are present in the reference. This is caused by the camera's technology limitations, as it does not have enough spectral resolution to capture them, and there is some crossband interference due to the filtering technology. Also, there is an offset in the reflectance between the different signatures. It is not very relevant as it can be caused due to some differences in the illumination system and is inherent in most of the HS images.

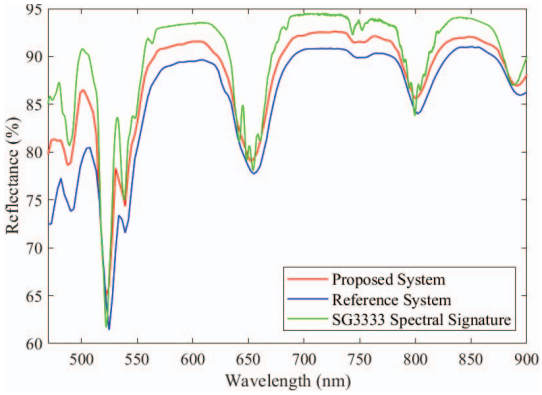

Fig. 8. Certified spectral signature of Zenith Polymer SG3333 (green) and average spectral signatures using the proposed system (red) and the reference HS camera system (blue).

For comparing with precision if the colposcope introduces any aberration, the Root-Mean-Square Error (RMSE) was computed between the reference camera system and the HS colposcope developed in this work. As seen in the Fig. 8, there was an offset in the reflectance between the spectral signatures captured for both systems. The impact from the offset was diminished by eliminating the DC component in both signatures, as shown in Fig. 9. Then, the RMSE was computed, achieving a value of 0.0168. This result confirms the visual impression that there is a slight error between them. When both signatures are compared with detail, it is noticeable that the most significant error is introduced in the range of 470 to 520 nm and from 840 to 900 nm. These areas are the limits of the camera's capture range, where it has a noticeable lower sensitivity due to technological limitations.

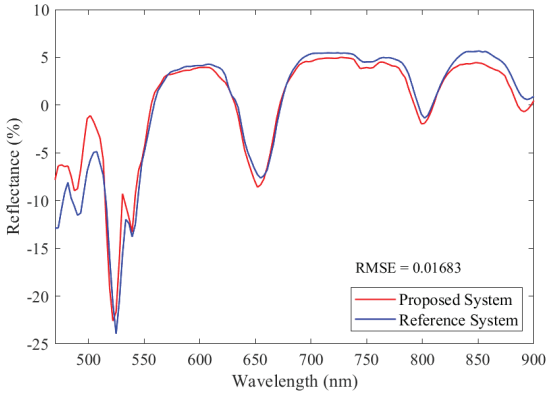

Fig. 9. Calculation of RMSE between spectral signatures after removing the DC component of both.

Furthermore, Fig. 10 shows the HS image of the SG3333 captured with the HS colposcope. There are different areas marked on the image (Fig. 10.A) that have their corresponding spectral signature (Fig. 10.B), ordered by their distance from the centre of the image. This comparison reveals that inside the field of view area (red, blue and green squares) there is not a noticeable distortion in the spectrum, the only difference is that the central area (red) and P1 (blue), have a peak in 630 nm due to a reflection caused by the illumination system. On the area where P3 (cyan) was selected, instead, the spectral signature is noisy due to it is located outside the limit of vision of the colposcope.

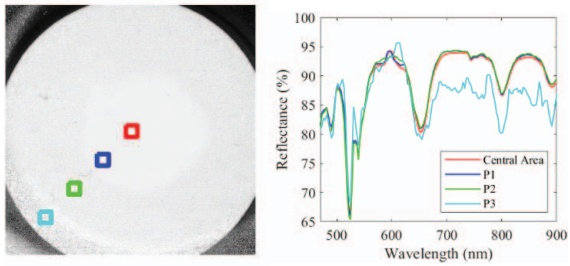

(A) (B)

Fig. 10. Spectral deformation in different areas of an HS image of the SG3333 captured with the HS colposcope. (A) Image of SG3333 with each area marked and (B) Spectral signature in each area.

2) Experiment with the White Reference

These previous results are based on the reflectance measure, which is a value calculated relative to the white reference, and it is not affected as much by the environment and the acquisition system employed. As the goal is to ensure that the error introduced by the proposed system is as low as possible, it was necessary to have a final analysis with a direct metric from the captured results.

Fig. 11 shows a comparison between the raw values of the white reference captured by both systems. Under ideal conditions, the white reference must have a constant value as it reflects the spectrum neutrally. In reality, the value for each band depends on the sensor's sensitivity to each wavelength, the lenses' spectral response and the type of light that is used by the system. For the IMEC's sensor, the expected figure has peaks and valleys, with maximum sensitivity at 590 nm and a lower range between 620 and 660 nm. It should also have some relevant peaks at 690, 720 and 750 nm, while on the limits of the spectral acquisition range it is not especially sensitive.

In Fig. 11 can be seen that over 800 nm, there is a noticeable difference between both signals. These differences are produced by the prism that divides the image inside camera splitter. For dividing the image, is used a non-polarizing cube beamsplitter which is designed for having an operational range in the Visible Spectrum (VIS) range (400 to 700 nm). The progressive loss in the transmittance over 700 nm explains the flattening of the spectral signature in the proposed system, compared to the reference setup that has the highest value in 850 nm. Although this issue is not ideal, it is acceptable because the halogen light source used has its highest spectral emission in the 900 nm band and compensates the reduction in the transmission of the prism.

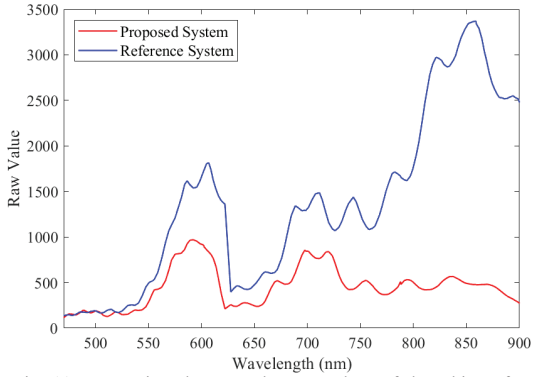

Fig. 11. Comparison between the raw values of the white reference captured by both systems.

3) Experiment Distorsion Target

Finally, the distortion target was captured to compare any spatial deformations introduced in the image. Fig. 12 shows the HS images obtained with the proposed system on the right (B) and the reference one on the left (A). Due to the nature of the colposcope system, the image area has a rounded format as it is equivalent to the one visible in the binocular. In the reference HS camera system (Fig. 12.A), there is no visible deformation in the target with the images captured at a distance between the lens to the object of 260 mm. In the image captured with the proposed system (Fig. 12.B), it is clearly noticeable a barrel distortion aberration which affects more the outer area of the image. Also, there is an offset between the centre of the projected image and the sensor's centre. This second deformation can be corrected because the view area is 1200 × 1200 pixels, while the camera has an area of 3600 × 2048 pixels, so the captured area can be offset 93 pixels to the left and 121 pixels to the bottom for centring the image.

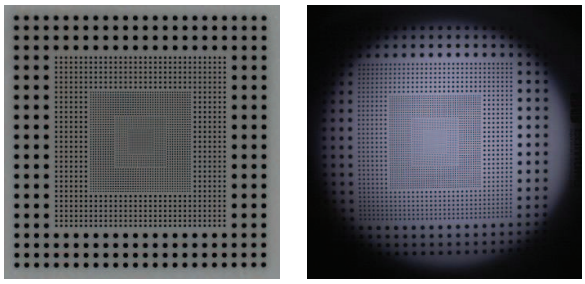

(A) (B)

Fig. 12. Spatial deformation comparison results using the distortion target. (A) HS images captured using the reference HS camera system and (B) the HS colposcope.

B. Comparison of acquisition time

For integrating this solution into a medical environment, it is necessary to have a capture time as low as possible. This will reduce the inconveniences of having an additional tool in the workflow during consultation. The reference system uses an external illumination composed of four halogen bulbs with a combined maximum power of 119 W. In contrast, in the HS colposcope, the system is connected to an external halogen light source of 150 W by using a fibre optic light guide. At first, this solution seems powerful enough, but as there are important differences in the optics it must be evaluated.

Four images were taken to assess the impact in the capturing time of the HS colposcope respect to the reference camera system. Both images were captured with the illumination at their maximum power output. Fig. 13 shows the total acquisition time of each image with brightness level in the results. Those images captured two different configurations of the Time Delay Integration (TDI) pixel step, which defines how many steps the sensor moves between each image.

With a TDI pixel step of 1, the acquisition times are too long for this use case, with a time of 128.7 s for the reference system and up to 205 s for the HS colposcope. Setting the TDI pixel step to 5, the time is significantly reduced to 2.95 s for the reference system and 40.35 s for the HS colposcope.

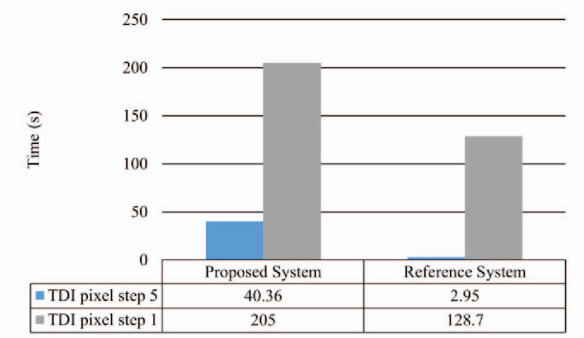

Fig. 13. Acquisition time of each capture system.

These results indicate a large reduction in capturing the samples with a TDI pixel step of 5. The alteration of this parameter affects to the band-to-band crosstalk, which in theory could reduce the ability of detecting specific spectral footprints in the image. Fig. 14 shows a comparison of the spectral signatures of the Polymer SG3333 captured with a TDI step pixel of 1 (red) and 5 (blue). The results show that for our conditions there is not relevant impact on the signature, since apart from minor variations, both are able to capture the peaks and valleys of the polymer's spectral signature without much difference between them.

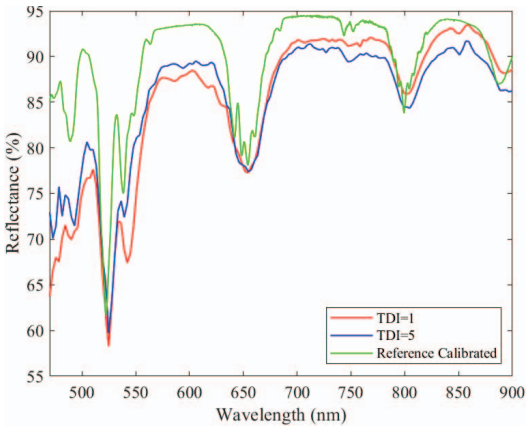

Fig. 14. Comparison of the spectral signature of SG3333 captured under different TDI step pixel configurations.

Even after setting TDI step pixel to 5, the HS colposcope presents an increase in the HS image acquisition time of 13.7× over the reference system. This issue happens due to the combination of 3 different situations. First, the image is magnified compared to the reference system, which causes the sensor to capture the reflected light of a smaller area. Second, the beamsplitter prism reduces the amount of light received by 50%, as the rest of the incoming light is redirected to the binoculars. Also, it is rejecting a higher percentage of light over 700 nm, as it is outside its operational range. Finally, the issue with the focal distance also affects the amount of light received by the HS camera sensor, requiring incrementing the integration time for the image acquisition.

C. Discussion

The captured results do not show a significant impact in the spectral performance of the proposed HS colposcope compared to the reference system setup. The results with the Zenith Polymer SG3333 confirmed that no deformation was introduced, with an RSME of 0.01683 between the spectral signatures.

The most significant limitation is the increment in the acquisition time, which is currently 13.7 times longer than using the reference system. This problem is a primary consequence of the colposcope image splitter. As analysed, the HS camera only receives 50% of the incoming light and this percentage is lower for the bands over 700 nm. This disadvantage is accentuated due to the coupling issue between the splitter and the HS camera.

The splitter is designed for a camera body with the standard CS-mount, which has a flange focal distance of 12.526 mm, while the HS camera uses the standard C-mount. The C-mount is equivalent to the first one, but it has a flange focal distance of 17.526 mm. This causes the captured image to have a darker exposure, a narrower view angle and a larger zoom, and the focus area gets displaced closer. This effect has been noticed in practice as the focal range of the colposcope has been moved closer after adjusting to the camera's focal offset.

None of these inconveniences represents a severe problem for the goals of the project, as they can be solved in the future with slight modifications in the optics of the splitter. Additionally, future experiments will be carried out to quantify the spatial distortions of the HS images introduced by the colposcope optics.

IV. Conclusions

This work aims to introduce to the gynaecologist a new tool based on HS images for detecting and classifying cervical neoplasia in routine medical check-ups and precisely define its extension. The presented work is the first stage in developing this tool, but the goal is to introduce this technology as an easy-to-use diagnostic support tool in the current physician's workflow.

The primary tool in the current detection process is the colposcope, which allows gynaecologists to detect any abnormal region in the cervix with high detail. This made it an ideal device to include the HS camera needed for this project.

The results obtained during the validation process were promising and showed that integrating an HS camera with a colposcope is a feasible task. The inconveniences found when using the current image splitter with the camera are not critical for the first stage of development and validation. However, they are expected to be solved in further developments.

Also, the developed software for this project has simplified the capture process and reduced the interaction needed with the computer by at least 50% once the system has been set up. It is easy to explain for the medical doctors and will speed up the capturing process in the first stage of creating a dataset of clinical HS images.

In conclusion, this work opens new possibilities for developing future tools for the screening and early detection of cervical neoplasia and cervical cancer. After reviewing the state of the art, it is clear that HSI is a promising technology to improve the recognition of these pathologies. The next step is to start the creation of a dataset with HS captures from gynaecological patients for the development of new algorithms able to exploit the possibilities HSI for this application.

ACKNOWLEDGMENT

This work was completed while Carlos Vega García and Raquel Leon were a beneficiary of a pre-doctoral grant given by the Agencia Canaria de Investigacion, Innovacion y Sociedad de la Información (ACIISI) of the Consejería de Economía, Conocimiento y Empleo, which is part-financed by the European Social Fund (FSE) (POC 2014- 2020, Eje 3 Tema Prioritario 74 (85%)) and, Himar Fabelo was beneficiary of the FJC2020-043474-I funded by MCIN/AEI/10.13039/501100011033 and by the European Union NextGenerationEU/PRTR. This work has been partially supported also by the Spanish Government and European Union (FEDER funds) as part of support program in the context of TALENT-HExPERIA (HypErsPEctRal Imaging for Artificial intelligence applications) project, under contract PID2020-116417RB-C42. Also, the cooperation of OPTOMIC is gratefully acknowledged for the donation of the Colposcope, used for the development of the proposed system, and their technical support.

REFERENCES

[1] "Global Cancer Statistics 2020," 2020. Accessed: May 16, 2022. [Online]. Available: https://gco.iarc.fr/today

[2] F. Bray, J. Ferlay, I. Soerjomataram, R. L. Siegel, L. A. Torre, and A. Jemal, "Global cancer statistics 2018: GLOBOCAN estimates of incidence and mortality worldwide for 36 cancers in 185 countries," *CA: A Cancer Journal for Clinicians*, vol. 68, no. 6, pp. 394–424, Nov. 2018, doi: 10.3322/caac.21492.

[3] A. Herrera *et al.*, "Estimaciones de la Incidencia de Cáncer en Canarias 2018," 2018.

[4] Jan M. Walboomers *et al.*, "Human papillomavirus is a necessary cause of invasive cervical cancer worldwide," *J. Pathol*, vol. 189, pp. 12–19, 1999, doi: 10.1002/(SICI)1096-9896(199909)189:1.

[5] A G Ostör, "Natural history of cervical intraepithelial neoplasia: a critical review," *International Journal of Gynecological Pathology*, 1993.

[6] P. Hillemanns, P. Soergel, H. Hertel, and M. Jentschke, "Epidemiology and Early Detection of Cervical Cancer," *Oncology Research and Treatment*, vol. 39, no. 9, pp. 501–506, 2016, doi: 10.1159/000448385.

[7] M. Prakash, S. Patterson, and M. S. Kapembwa, "Evaluation of the cervical cytobrush sampling technique for the preparation of CD45+ mononuclear cells from the human cervix," *Journal of Immunological Methods*, vol. 258, no. 1–2, pp. 37–46, Dec. 2001, doi: 10.1016/S0022-1759(01)00464-1.

[8] N. Wentzensen *et al.*, "A prospective study of risk-based colposcopy demonstrates improved detection of cervical precancers," *American Journal of Obstetrics and Gynecology*, vol. 218, no. 6, pp. 604.e1-604.e8, Jun. 2018, doi: 10.1016/j.ajog.2018.02.009.

[9] D. M. Chase, M. Kalouyan, and P. J. DiSaia, "Colposcopy to evaluate abnormal cervical cytology in 2008," *American Journal of Obstetrics and Gynecology*, vol. 200, no. 5, pp. 472–480, May 2009, doi: 10.1016/j.ajog.2008.12.025.

[10] J. Walker, "A randomized trial on the management of low-grade squamous intraepithelial lesion cytology interpretations," *Am J Obstet Gynecol*, vol. 188, no. 6, pp. 1393–1400, Jun. 2003, doi: 10.1067/MOB.2003.462.

[11] R. G. Pretorius *et al.*, "Colposcopically directed biopsy, random cervical biopsy, and endocervical curettage in the diagnosis of cervical intraepithelial neoplasia II or worse," *American Journal of Obstetrics and Gynecology*, vol. 191, no. 2, pp. 430–434, Aug. 2004, doi: 10.1016/J.AJOG.2004.02.065.

[12] R. Guido, M. Schiffman, D. Solomon, and L. Burke, "Postcolposcopy management strategies for women referred with low-grade squamous intraepithelial lesions or human papillomavirus DNA-positive atypical squamous cells of undetermined significance: a two-year prospective study," *Am J Obstet Gynecol*, vol. 188, no. 6, pp. 1401–1405, Jun. 2003, doi: 10.1067/MOB.2003.456.

[13] M. Kamruzzaman and D. W. Sun, "Introduction to Hyperspectral Imaging Technology," *Computer Vision Technology for Food Quality Evaluation: Second Edition*, pp. 111–139, Jan. 2016, doi: 10.1016/B978-0-12-802232-0.00005-0.

[14] Y. N. Mirabal, S. K. Chang, E. N. Atkinson, A. Malpica, M. Follen, and R. Richards-Kortum, "Reflectance spectroscopy for in vivo detection of cervical precancer," *J Biomed Opt*, vol. 7, no. 4, p. 587, 2002, doi: 10.1117/1.1502675.

[15] A. M. J. Wang, V. Nammalvar, and R. A. Drezek, "Targeting spectral signatures of progressively dysplastic stratified epithelia using angularly variable fiber geometry in reflectance Monte Carlo simulations," *https://doi.org/10.1117/1.2769328*, vol. 12, no. 4, p. 044012, Jul. 2007, doi: 10.1117/1.2769328.

[16] C. Wang, W. Zheng, Y. Bu, S. Chang, S. Zhang, and R. X. Xu, "Multi-scale hyperspectral imaging of cervical neoplasia," *Arch Gynecol Obstet*, vol. 293, no. 6, pp. 1309–1317, Jun. 2016, doi: 10.1007/S00404-015-3906-8.

[17] M. Halicek, H. Fabelo, S. Ortega, G. M. Callico, and B. Fei, "In-Vivo and Ex-Vivo Tissue Analysis through Hyperspectral Imaging Techniques: Revealing the Invisible Features of Cancer," *Cancers (Basel)*, vol. 11, no. 6, p. 756, May 2019, doi: 10.3390/cancers11060756.

[18] "SNAPSCAN VNIR hyperspectral camera | imec." https://www.imechyperspectral.com/en/cameras/snapscan-vnir (accessed May 16, 2022).

[19] J. Pichette, W. Charle, and A. Lambrechts, "Fast and compact internal scanning CMOS-based hyperspectral camera: the Snapscan," Feb. 2017, p. 1011014. doi: 10.1117/12.2253614.